The Journal of the Korean Society of
Coastal and Ocean Engineers
Vol. 6, No. 1, pp. 51~60, March 1994

One-D Model Prediction of Pollutant Transport at a Canal Network
水路網에서의 汚染物質 擴散의 1次元 豫測

Jung Lyul Lee* and Hsiang Wang**
이정렬* · 시앙왕**

Abstract □ A one-dimensional numerical model has been developed through a Lagragian formulation, which is applicable to advection and diffusion of dissolved matters in storages. The study was conducted to the pollutants released into a canal network in Burnt Store Isles, Punta Gorda, Florida, USA. The hydrodynamic model was developed by using an implicit finite difference scheme. In the computational domain, the network system consists of prismatic channels and storages. The finger canals and small tributaries are treated as storages in the simplified flow network. The numerical results show relatively good agreement with field experiments.

要 旨 : 여유고에서 오염물질의 이동과 확산을 효율적으로 모의할 수 있는 Lagragian 기법을 이용한 1차원 수치모델이 개발되어 미국 플로리다주의 Burnt Store Isles의 수로망(canal network)으로 유입되는 오염물질에 대해서 적용되었다. 본 수력학 모델은 음해법으로 수치해석되었다. 수치 영역은 크게 主水路와 여유고(storage)로 대별되며 指水路(finger canal)와 支流(tributary)들은 수로망을 단순화하기 위하여 여유고로 간주되었다. 수치실험 결과는 현장실험결과와 비교하여 비교적 잘 일치하고 있음을 보여준다.

1. INTRODUCTION

The boat lock where the study was conducted is located in Section 15, Burnt Store Isles, Punta Gorda, Florida, USA. This Section consists of residential subdivisions along a canal network and a golf course country club (Figure 1). Practically all the residential units are fronted with canals. As can be seen in the figure, all the finger canals eventually enter a main trunk which forms a belt around in the figure, the western boundary of the subdivision.

For concerns about pollutants from the canal network being carried into the Alligator Creek through the lock, it is currently allowed to open only during the period of November 15 to May 15 when the discharge is thought to be small. During the remaining six months the lock is kept closed and boat transits have to pass through the normal lock operation. This is not only inconvenient to the boaters but also adds financial burden to the City of Punta Gorda for lock maintenance. The main purpose of this study is to estimate pollutant transports through the lock in comparison with the amount by-passing the lock by transport through the other outlets. As a proper model to solve it, the one-dimensional water quality model was selected which has been believed to be easily applicable to the canal network.

2. MODEL DESCRIPTION

A one-dimensional numerical model was developed for this study. The major purpose of the model is to argument the field data for estimation of discharges at various points in the study area and to assess the dispersion characteristics at the boat lock. The computational domain and grid point system

*韓國海洋研究所 博士後 課程 (Ocean Engineering Division, Korea Ocean Research and Development Institute, Ansan P.O. Box 29, 525-600, Korea)
**플로리다 大學 海岸·海洋工學科 (Coastal and Oceanographic Engineering Department, University of Florida, Gainesville, FL 32611, USA)

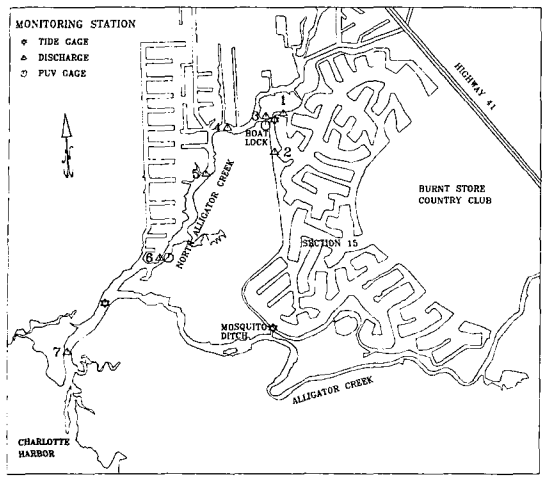

Fig. 1. Alligator Creek and Section 15, Burnt Store Isles, Punta Gorda, Florida, USA.

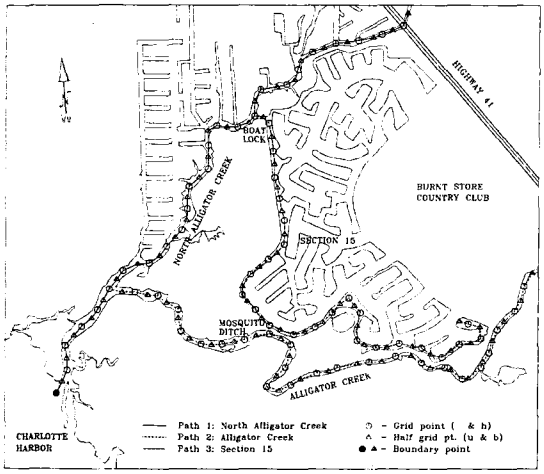

Fig. 2. Area and grid point system considered in the model.

of the model are given in Figure 2. The creek and trunk channels in the computational domain is actually described by a simplified flow network in the model. The network consists of prismatic channels representing the Alligator Creek, the north branch of the Alligator Creek and the trunk canal portion in Section 15. The finger canals and small tributaries are treated as storages in the simplified flow network.

3. GOVERNING EQUATIONS

The one-dimensional equations of continuity, momentum and transport-diffusion are used as basic equations of the model to predict surface elevation (η), vertically-and laterally-integrated flow rate (Q) and vertically-and laterally-averaged concentration of any dissolved matter (c).

$$b\frac{\partial \eta}{\partial t}+\frac{\partial Q}{\partial x}-q=0 \tag{1}$$

$$\frac{\partial Q}{\partial t}+\frac{\partial uQ}{\partial x}+gA\frac{\partial \eta}{\partial x}+gb\frac{|u|u}{C^2}=0 \tag{2}$$

$$\frac{\partial Ac}{\partial t}+\frac{\partial Qc}{\partial x}-qc_l-\frac{\partial}{\partial x}\left(AK\frac{\partial c}{\partial x}\right)=0 \tag{3}$$

where, u is the vertically-and laterally-averaged velocity, q is the lateral influx, g is the gravity acceleration, b is the channel width, A is the channel area, C is the Chezy coefficient, C_l is the concentration of lateral influx, and K is the dispersion coefficient. The Chezy coefficient is related to the Darcy-Weisbach resistance coefficient, f, by the formula $C=\sqrt{8g/f}$.

4. NUMERICAL SCHEME

4.1 Hydrodynamic Model

The process of transport and longitudinal dispersion of pollutants in the canal network mainly depends on the hydrodynamic characteristics of the flow. In the following, the numerical scheme of a one-dimensional hydrodynamic model is described. To solve Eqs. (1) and (2), an implicit finite difference method is used on the staggered grid system:

$$\frac{\eta_i^{n+1}-\eta_i^{n-1}}{2\Delta t}+\frac{1}{\overline{b}}\frac{(Ub)_i^{n+1}-(Ub)_i^{n+1}}{\Delta x}+\frac{q_s+q_b}{\overline{b}}=0 \tag{4}$$

$$\frac{U_i^{n+1}U_i^{n+1}}{2\Delta t}+g\overline{h}\frac{\eta_{i+1}^{n+1}-\eta_i^{n+1}}{\Delta x}+\frac{f|u_i^n|U_i^{n+1}}{8\overline{h}}=0 \tag{5}$$

where U is the depth integrated velocity, and $\overline{b}$ and $\overline{h}$ are the average width and depth, respectively; the subscripts s and b refer to storage and branch, respectively. The advective term in Eq. (2) is assumed to be negligible. Referring to Figure 2, the surface elevation, concentration and water depth are defined at grid points whereas the flux and width are given

at half-grid points. The storages and branches are connected at grid points, their elevations are assumed to be the same there. Assuming that the surface variation in the storage areas is instantaneous, Eq. (4) can be rewritten as

$$\frac{\eta_j^{n+1}-\eta_j^{n-1}}{2\Delta t}+\frac{1}{b}\frac{(Ub)_i^{n+1}-(Ub)_{i-1}^{n+1}}{\Delta x}-\frac{1}{b}\frac{\frac{S_i(\eta_i^{n+1}-\eta_j^{n-1})}{2\Delta t}+(Ub)_b}{\Delta x}=0 \tag{6}$$

where S is the surface area of storage. The above finite difference equations, Eqs. (6) and (5) are solved by implicit finite difference scheme forming a tridiagonal matrix. There are two kinds of boundary conditions as shown in Figure 2. One is the open boundary condition at sea end which is given as the recorded tidal history, and the other is the upstream boundary conditions which are specified as the influxes from rivers.

4.2 Water Quality Model

Several distinct numerical improvements have been made for the advection and diffusion of matter dissolved. The representive Eulerian schemes are the quadratic upstream interpolation for convective kinematic with estimated streaming terms (QUICKEST) scheme first presented by Leonard (1979) and the two-point fourth-order scheme by Holly and Preissmann (1977). However, any Eulerian scheme is not capable of handling the advection and diffusion of matter dissoved in the storages. Owing to this reason, the Lagrangian scheme was employed here.

After the continuity equation the momentum equation are solved, the transport equation (3) is solved by a Lagrangian formulation which takes the following term

$$\frac{Dc}{Dt}=K\frac{\partial^2 c}{\partial x^2} \tag{7}$$

where K is assumed to be constant and $D/Dt=\partial/\partial t+u\partial/\partial x$. Equation (7) is solved in two fractional steps at each time step: (i) by the transport of concentration elements due to convection, and (ii) by the random walk displacement of the same elements due to dispersion (Chorin, 1978; Chorin, 1980). The convection operator allows the displacement of each element by the velocity computed from the hydrodynamic model. Once the velocity is obtained, it is easy to have

$$x_j(t+\delta t)=x_j+u(x_j)\delta t$$

for jth element by using a first-order difference formula. The dispersion operator with an impulse as initial condition has a solution which is the probability density function of a Gaussian distribution with zero mean and a variance $2K\delta t$. Therefore, the dispersive transport of concentration elements is simulated by adding to their convective motion and additional random walk displacement drawn from a Gaussian distribution with zero mean and a variance $2K\delta t$. The total transport is obtained by adding the two fractional displacements.

$$x_j(t+\delta t)=x_j+u(x_j)\delta t+\xi_x \tag{8}$$

where the last term in the right hand side is for the random walk in the x (longitudinal) direction. The open boundary condition at sea end is assumed to be satisfied by a complete absorption without reflection. The upstream boundary conditions are satisfied by mirror-image method.

At the grid position with storage or branch, the concentration elements are assigned or put together according to the ratio of discharge flowing, and the position of elements moved into the new channel or storage is replaced by their own coordinates. The transport and diffusion in the storage are approximated by using the following lateral coordinate, y, which is originated from each storage entrance:

$$y_j(t+\delta t)=y_j+u_s(x_j)\delta t+\xi_y \tag{9}$$

where $u_s(x_j)$ denotes the velocity entering into the storage where a concentration element is located, and the last term in the right hand side is for the random walk in the y (lateral) direction. When y in Eq. (9) becomes a negative value, the position is transfered back to the x coordinate.

5. APPLICATION OF MODEL

5.1 Field Measurements

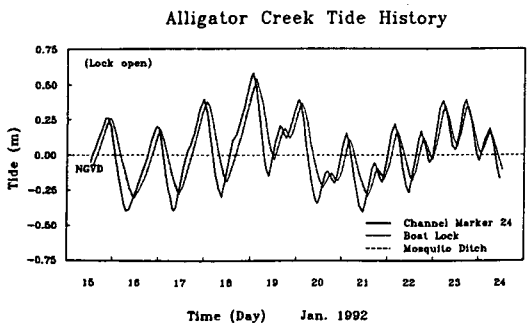

Fig. 3. Tidal histories measured during the winter experiment.

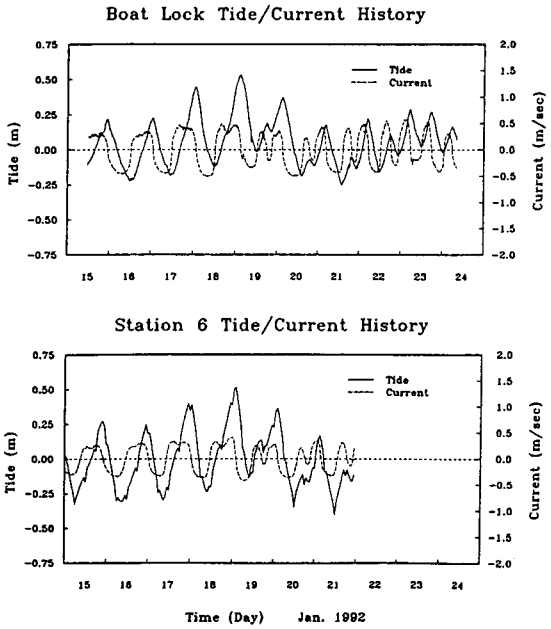

Fig. 4. Water surface and current measurements at the boat lock and Station 6.

Field measurements were conducted during the winter from January 15th to 24th, 1992. As shown in Figure 1, three tide gages and two PUV gages were installed and current elocing measurements were carried out at seven cross-sections designated as Stations 1 to 7. Dispersion studies were also carried out at the lock. The experiment was performed by injecting the Rhodamine dye at the lock at the beginning of the flood tidal cycle on January 21st and continuously monitoring its concentrations for a duration of two days.

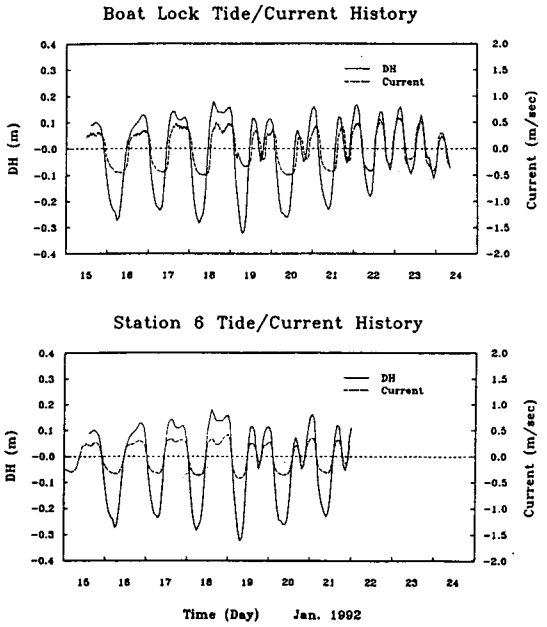

Fig. 5. Plots of measured currents versus head differences.

The tide gages were put in operation just before the arrival of a spring tidal cycle. The water surface fluctuation histories at the three locations are shown in Figure 3. The nature of the tide was almost purely diurnal during the first half of the eight-day recording and then gradually turned into a mixture of diurnal and semi-diurnal. Tidal ranges were larger when diurnal component dominated. The PUV gages at the lock location and at Station 6 yielded simultaneous water surface and current records and they are presented in Figure 4. The PUV gage measurements showed that the currents are fairly well behaved and are governed mainly by the tidal elevation differences between upstream and downstream. This situation is illustrated in Figure 5 by plotting the current velocity measured together with the tidal differences between boat lock and Channel Marker 24. The current measurements taken at individual cross-sectional stations, in general, consisted of three vertical profiles, each with two to three depth levels depending upon the water depth. Based on these measurements the flow discharges, Q, through individual stations are computed. Figure 6 plots the discharge against the water level difference, ΔH, between the lock and Channel Marker 24. The

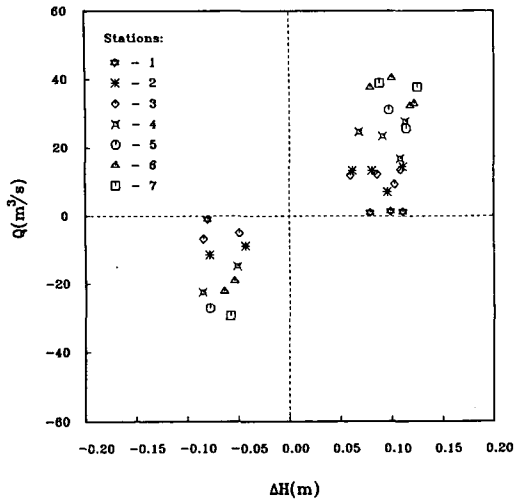

Fig. 6. Plot of discharge versus head difference.

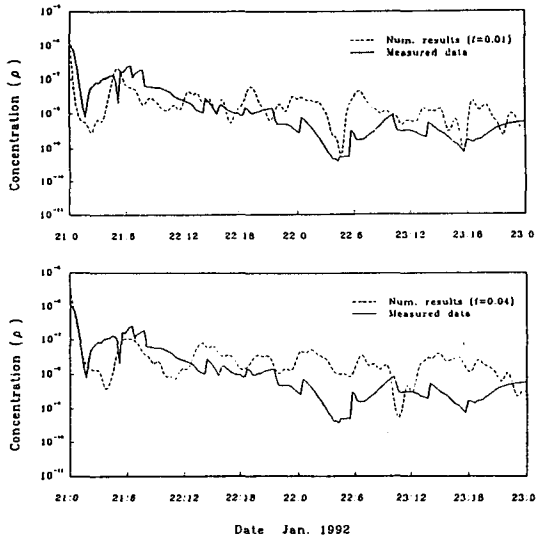

Fig. 7. Plot of concentration of Rhodamine dye versus time.

positive Q indicates flow up to the creek from the Charlotte Harbor and negative Q corresponds to flow downstream towards the Harbor.

The results of the dye dispersion test are presented in Figure 7 by plotting the concentration of Rhodamine in ppm, log ρ, versus time, monitored at the lock.

5.2 Calibration of Hydrodynamic Model

The hydrodynamic model requires the determi-

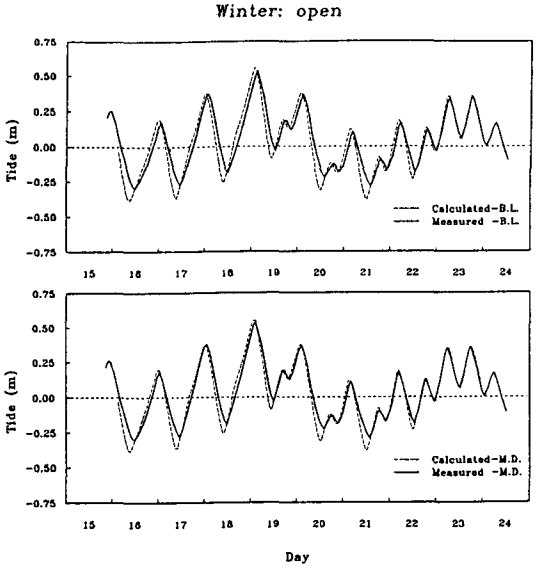

Fig. 8. Comparison of computed and measured surface elevations.

nation of one empirical coefficient, namely, the Chezy coefficient, C, or its equivalent Darcy-Weisbach friction coefficient, f. This was accomplished by adjusting the numerically simulated water surface and current time series to match those of the measured ones. Based upon the criterion of the best overall agreement, the optimum value of the friction coefficient was determined to be $f=0.04$. Figures 8 and 9 show the comparisons between the calculated and measured ones of surface elevation and currents, respectively, using $f=0.04$. The numerical results shown in Figure 9 were fitted for time-serial traces.

5.3 Estimation of Dispersion Coefficient

The longitudinal dispersion coefficient, K, used in the transport model was determined by comparing the simulated concentration variations with that measured at the boat lock (Figure 7). The optimum value of K was determined to be about 0.8 m^2/s for the trunk canal. This value appears to be reasonable for channels of narrow width but could be too small at the creek (Fisher *et al.*, 1979). Nevertheless, the K value is kept constant in the numerical simulation.

5.4 Prediction of Flow and Discharges

The simulated discharge time series was integra-

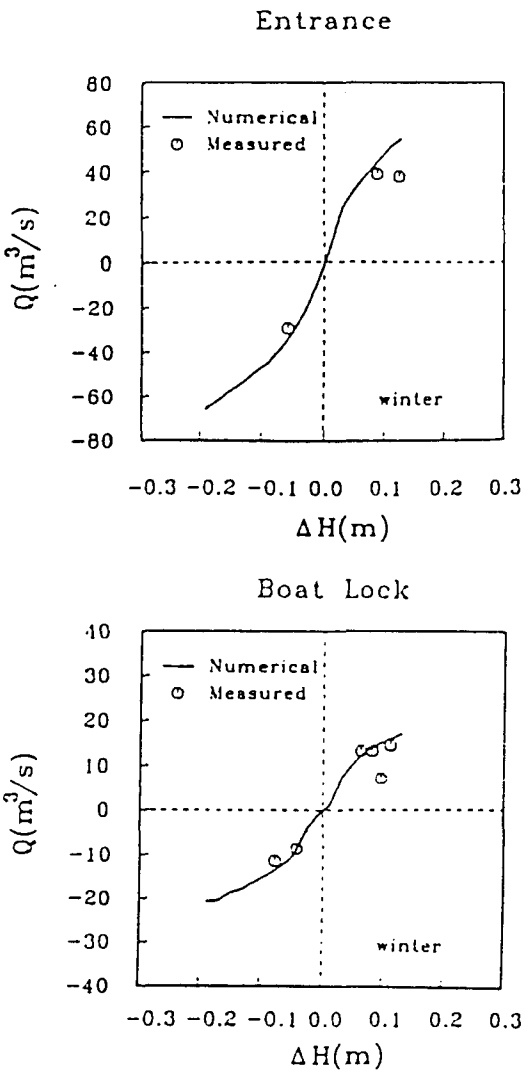

Fig. 9. Comparison of computed and measured flow currents.

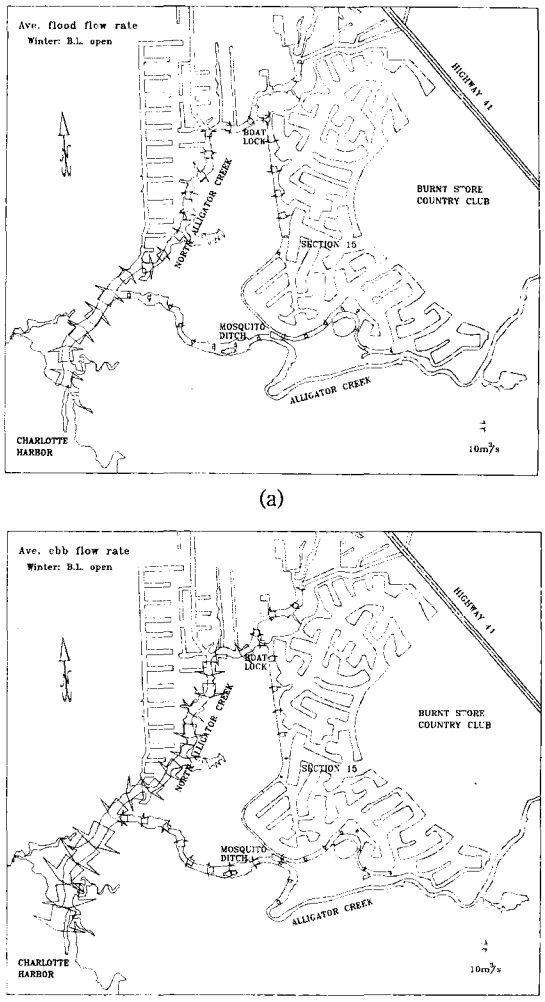

Fig. 10. Time-averaged flow pattern under lock-open condition.

ted to obtain the time averaged quantities. Depending upon the nature of the integrands, a number of different quantities can be established:

1. Average flood flow rate: $\overline{Q}_f = \frac{1}{T_f}\int_0^{T_f} q_f dt$

2. Average ebb flow rate: $\overline{Q}_e = \frac{1}{T_e}\int_0^{T_e} q_e dt$

where q is the instantaneous flow rate; T is the period of recording. The subscripts e and f refer to ebb and flood, respectively.

Figure 10a plots the flow vectors for the average flood flow rate with the boat lock open and Figure 10b plots the average ebb flow rate under the same condition. These plots provide us with a visual display on the flow pattern as well as the magnitudes of the flow rate. The exchange through the lock opening is 33% whereas the exchanges through the mosquito ditch and the north opening are 17% and 5%, respectively. Therefore, the sum of these three which represents the bulk of exchange between Section 15 and the creek system amounts to 55%.

The second simulation is for lock-closure condition using the measured 8-day tidal record as input.

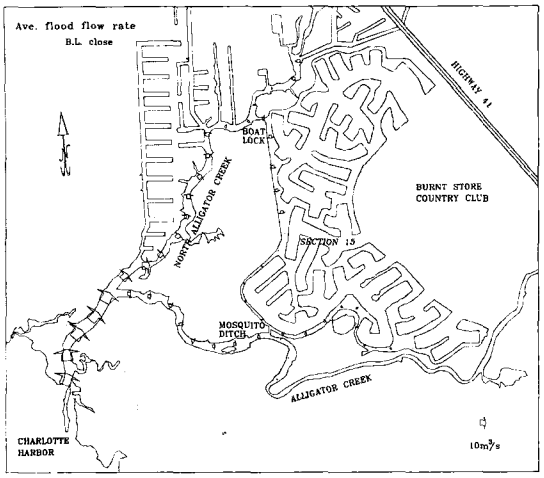

(a)

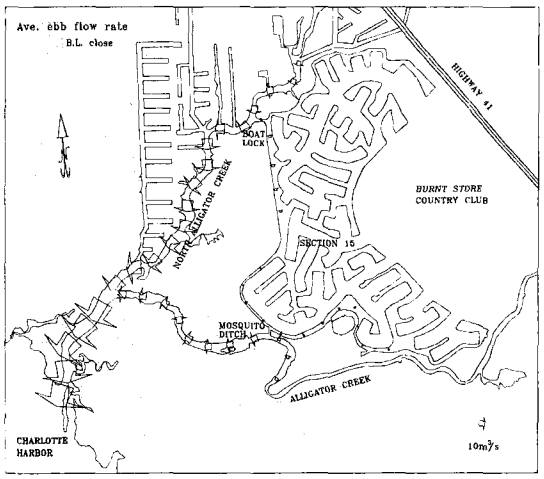

(b)

Fig. 11. Time-averaged flow pattern under lock-closed condition.

Since the lock is not completely water tight, a 85% closure is used allowing for the leakage through the bottom and the sides. For the lock-closed condition, the flow rate is reduced but flow pattern remains the same as the lock-open condition as shown in Figure 11. The exchange through the lock, the mosquito ditch and the north opening are 18%, 26% and 9%, respectively for the total value of 53%, whereas the exchanges through the mosquito ditch and the north opening are 17% and 5%, respectively. Therefore, the sum of these three which represents the bulk of exchange between Section 15 and the creek system amounts to 55%.

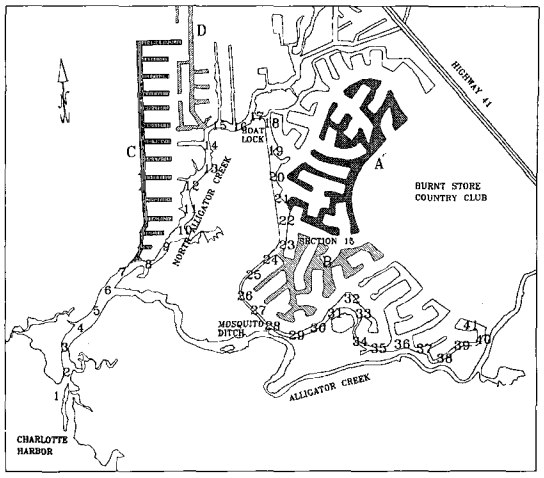

Fig. 12. Regions affected by pollutant from Section 15.

5.5 Pollutant Transport

The main purpose of this study is to examine whether the closure of the lock will effectively contain the pollutant within the canal network in the Section 15. Pollutant in the water column will be transported through current convection and turbulent diffusion; the magnitude and pattern of the tidal current were already established and the diffusion property in the lock vicinity was examined by a simple dye study. As discussed earlier, based on the results of the dye study and the one-dimensional transport numerical model, the longitudinal diffusion coefficient in the trunk canal was established as equal to 0.8 m^2/s. The value might be slightly higher in the creek system.

Based upon numerical model simulations, pollutant passing through the lock section mainly affects the region shown as the shaded area in Figure 12. It includes two storage areas A and B in Section 15, two storage areas C and D outside along the north branch of the creek and the creek system itself. More detailed locations are marked on the map as grid location numbers from 1 to 41. The location #1 is at the entrance of the channel to the Harbor and location #41 is at the extreme south end of the trunk canal in Section 15. The grid locations #22 and #23 are the outlets of storages A and B, respectively, whereas #8 and #15 are the outlets for C and D, respectively.

Simulations were carried out for diurnal and

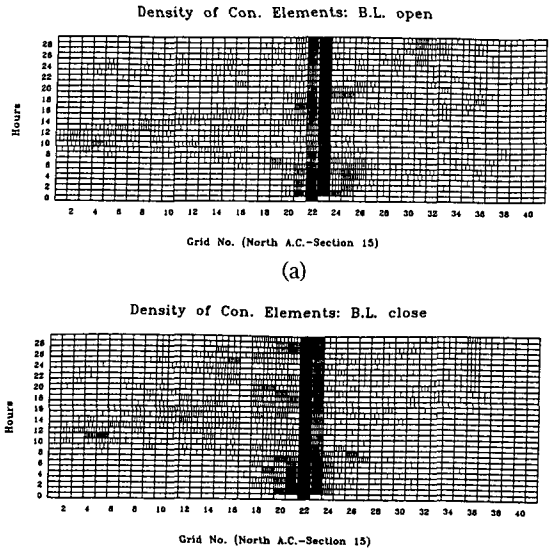

Fig. 13. Temporal and spatial variation of pollutant concentration under flood condition.

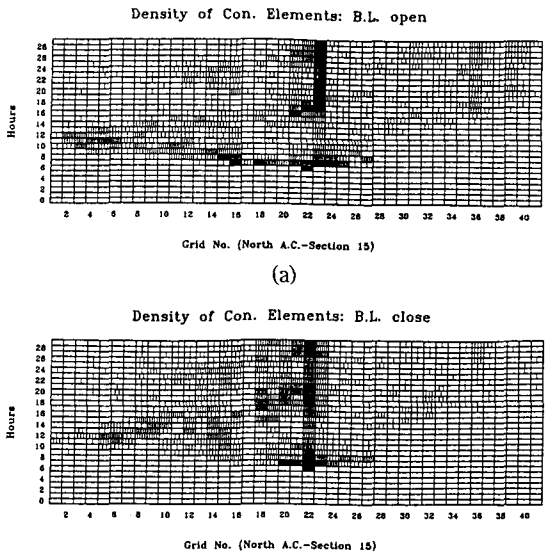

Fig. 14. Temporal and spatial variation of pollutant concentration under ebb condition.

semi-diurnal conditions with the lock open and with the lock closed. Some results for semi-diurnal tides are given here to explain the phenomenon. Since the main concern here is for pollutant originated from and in Section 15, the simulations are for pollutants released at a location #22 which represents those from a region A.

Figure 13a shows the tracing of the pollutant for lock-open condition from the beginning of a flood tide. In the graph, the abscissa plots the grid locations from #1 to #41 with distance between two neighbouring locations equal to 0.5 km; the ordinate is the time with origin sets at the beginning of the flood tide. Thus, the six-hour mark roughly represents the end of the flood and the beginning of the ebb for the semi-diurnal condition and so on. The lines in each grid represents the percentage of pollutant at a specific location and time. Therefore, the darker the shade the higher the percentage. For pollutant originating from region A (#22), it is largely trapped in the trunk canal and storages A and B during flood. A small amount moves further southward through the mosquito ditch into the Alligator Creek. When the flow changes its direction in the ebb cycle, a portion of the pollutant is being released from the storage and carried out mainly through the lock. A significant portion of the pollutant is still trapped in the A and B. Diffusion appears to dominate convection in this portion of the canal as the flow is very slow. As a consequence the amount of pollutant escaped in the creek is small. At the end of the ebb, the centroid of the escaped pollutant reaches somewhere around location #4 which is about 1 km downdrift of the junction. A small portion of it enters into the Charlotte Harbor. As tide reverses to flood, the pollutant traces back to updrift with the main route following the north branch into Section 15. Therefore, the concentration in regions A and B increases periodically. Throughout the process, region B is the main trapping.

Figure 13b shows the lock-closed condition for pollutant release at the beginning of a flood. Because of the reduced flow, the trapping time within the canal is increased. The pollutant eventually escapes through underneath the lock. The centroid of the pollutant now does not transport as far and all the storage areas along creek begin to trap the pollutant. Thus, closing the lock manages to trap the pollutant inside Section 15 longer. The pollutant eventually escapes into the north branch. Since the flow slower than the lock-open case the pollutant

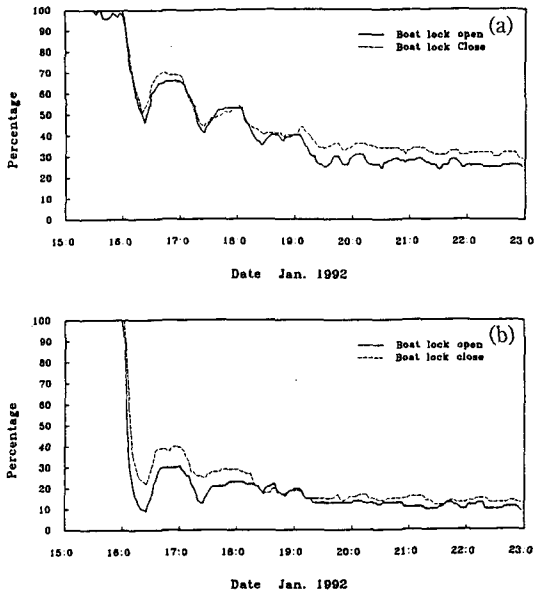

Fig. 15. Simulation of total pollutant dilution in Section 15.

now resides longer in the storage areas along the creek. Another effect of closing the lock is the increased transport through the mosquito ditch. This is evidenced by the appearance of two centroids along the creek near the end of ebb tidal cycle (10-12 hours). One centroid located upstream near locations #14 and #15 is due to the pollutant originating from the lock and the other centroid located downstream near the junction around #4 and #5 is due to the transport through the mosquito ditch. The total quantity escaped from Section 15 does not appear to have diminished significantly by closing the lock.

Now, for pollutant release at the beginning of ebb condition, Figure 14a shows the lock-open case. Here, the pollutant immediately transports into the Creek through the lock. The location of the centroid at the end of the ebb is roughly the same as the flood release but the concentration is now increased. As the flow reverses to flood the pollutant retraces its path back to Section 15. More pollutant is being trapped in storage areas along the creek. Again, Storage B is the main trapping of the system. For the lock-closed case (Figure 14b), the transport through the lock is delayed but the delay is not long enough to prevent the pollutant from eventually escaping to the creek before the ebb tide is over. The transport through mosquito ditch increases. Storage A now becomes the main trapping as stagnation zone in the trunk canal extends further north.

The total pollutant dilution in Section 15 for lock-open and lock-closed conditions are simulated using January tidal record as the input. The results are shown in Figure 15. The pollutant is released initially at location #22 at beginnings of flood (Fig. 15a) and ebb (Fig. 15b), respectively. For flood release, the pollutant initially disperses inside Section 15 while being trapped by the flood flow. Therefore, the rate of dilution is slower. For ebb release, the pollutant is being transport out of Section 15 considerably faster than the flood release case. The lock-open and lock-closed conditions, on the other hand, have only minor influence on pollutant transport in Section 15.

Like the flow exchanges, the boat lock is mainly responsible for pollutant exchanges from the central zone of Section 15 to the north branch of the Alligator Creek. The two end zones have different outlets. The flow exchanges among three zones are minor in single tidal cycle. The diffusion process, of course, eventually produces mixing of pollutants originating from different locations.

6. CONCLUSION

A one-dimensional model for describing the transport and diffusion of pollutants in the canal network has been developed. Model simulation successfully reproduces measured pollutant concentration and based on the study results, the boat lock is ineffective of trapping pollutant within Section 15. The reduction of pollutant transport is largely made up by the increased transport from the mosquito ditch. Closing the boat lock will likely to increase the average resident time of pollutant in the storage areas along the creek and to cause the pollutant to transport further upstream along the north branch. The storage areas (finger canal sections) and portion of the trunk canal are rather stagnant, thus, conducive to pollutant trapping. The above conclusions are based on a small amount of field data

collected under normal winter conditions. The numerical model is based on simplified assumptions and limited calibrations. Therefore, the results should be viewed within this context.

The numerical results revealed that the entire system is a sensitive one. Variations of input conditions or alternation of outlets could result in significant changes of flow conditions as well as the pollutant patterns. As an example, Storage B is the main trapping segment under lock-open condition. Under lock-closed case, the entire Section 15 is readjusted causing increased flow from other openings and the main trapping area shifted to storage A.

REFERENES

Chorin, A.J., 1978. Vortex sheet approx. of boundary layers, *J. Compt. Phys.*, **27**, 428-442.

Chorin, A.J., 1980. Vortex models and boundary layer instability. *SIAM J. of Sci. Stat. Compt.*, **1**, 1-21.

Fisher, H.B., List, E.J., Koh, R.C.Y., Imberger, J. and Brooks, N.H., 1979. *Mixing in inland and coastal waters.* Academic Press, New York, N.Y.

Holly, F.M., Jr., and Preissmann, A., 1977. Accurate calculation of transport in two dimensions, *Proc. AASCE, J. Hydraul. Div.*, **103**, 1259-1277.

Leonard, B.P. 1979. A stable and accurate convective modelling procedure based on quadratic upstream interpolation, *Comput. methods appl. mech. eng.*, **19**, 59-98.